Biochemical and Biophysical Research Communications 439 (2013) 351–356

Contents lists available at ScienceDirect

Biochemical and Biophysical Research Communications

journal homepage: www.elsevier.com/locate/ybbrc

Structure of native oligomeric Sprouty2 by electron microscopy and its property of electroconductivity

Feng-Jung Chen [a,b,1], Kuan-Wei Lee [a,1], Chun-Chieh Lai [a,1], Sue-Ping Lee [c], Hsiao-Hsuian Shen [a], Shu-Ping Tsai [c], Bang-Hung Liu [a], Ling-Mei Wang [d], Gunn-Guang Liou [a,e,*]

[a] Institute of Molecular and Genomic Medicine, National Health Research Institutes, Miaoli 35053, Taiwan, ROC
[b] Department of Photonics & Institute of Electro-Optical Engineering, National Chiao Tung University, Hsinchu 30010, Taiwan, ROC
[c] Institute of Molecular Biology, Academia Sinica, Taipei 11529, Taiwan, ROC
[d] Biomedical Engineering Research Laboratories, Industrial Technology Research Institute, Hsinchu 31040, Taiwan, ROC
[e] Graduate Institute of Basic Medical Science, China Medical University, Taichung 40402, Taiwan, ROC

ARTICLE INFO

Article history:
Received 22 August 2013
Available online 6 September 2013

Keywords:
Sprouty2 (Spry2)
Electron microscopy single particle reconstruction (EM SPR)
BIAcore surface plasmon resonance (BIAcore SPR)
Energy dispersive spectrum (EDS)
Electroconductivity

ABSTRACT

Receptor tyrosine kinases (RTKs) regulate many cellular processes, and Sprouty2 (Spry2) is known as an important regulator of RTK signaling pathways. Therefore, it is worth investigating the properties of Spry2 in more detail. In this study, we found that Spry2 is able to self-assemble into oligomers with a high-affinity KD value of approximately 16 nM, as determined through BIAcore surface plasmon resonance analysis. The three-dimensional (3D) structure of Spry2 was resolved using an electron microscopy (EM) single-particle reconstruction approach, which revealed that Spry2 is donut-shaped with two lip-cover domains. Furthermore, the method of energy dispersive spectrum obtained through EM was analyzed to determine the elements carried by Spry2, and the results demonstrated that Spry2 is a silicon- and iron-containing protein. The silicon may contribute to the electroconductivity of Spry2, and this property exhibits a concentration-dependent feature. This study provides the first report of a silicon- and iron-containing protein, and its 3D structure may allow us (1) to study the potential mechanism through the signal transduction is controlled by switching the electronic transfer on or off and (2) to develop a new type of conductor or even semiconductor using biological or half-biological hybrid materials in the future.

© 2013 Elsevier Inc. All rights reserved.

1. Introduction

Receptor tyrosine kinases (RTKs) regulate many fundamental cellular processes, including apoptosis, chemotaxis, differentiation, migration, proliferation, and survival [1–7]. The activated RTKs attract various signaling transducers to transmit a signal from the membrane to the nucleus through a signaling pathway, such as the MAPK cascade pathway [6–8]. RTK signal transduction plays an important role in many cellular processes; hence, these pathways must be temporarily and spatially tightly regulated. Sprouty (Spry) proteins are known as important regulators of RTK signaling in development and disease [4,9,10]. Therefore, a detailed understanding of the properties of Spry proteins is important.

It has been reported that the Sprouty2 (Spry2) protein regulates the RTK signal transduction through its interaction with several molecules of the RTK signaling pathways [4,9,10]. Nevertheless, the detailed mechanism is not yet fully elucidated. One of the regulatory mechanisms involves the binding of Spry2 to E3 ubiquitin ligases, such as Cbl (Casitas B-lineage lymphoma proto-oncogene), Siah2 (seven in absentia homolog 2), and Nedd4-1 (neuronal precursor cell-expressed developmentally down-regulated 4-1), which can then ubiquitylate Spry2 and target it for proteosomal degradation [4,9–16]. In addition, the epigenetic regulation of the Spry2 promoter and growth factors have been shown to modulate the transcription of Spry2 [17–19]. However, to investigate in more detail the biological role of spry2, the basic protein properties of Spry2 need to be further characterized.

In this study, yeast-derived recombinant Spry2 was purified through size-exclusion gel filtration following nickel-affinity chromatography. The purified Spry2 was further screened through negative-staining electron microscopy (EM) to assess the particle homogeneity and its suitability for subsequent three-dimensional (3D) structural reconstruction and further characterization.

* Corresponding author at: Institute of Molecular and Genomic Medicine, National Health Research Institutes, Miaoli 35053, Taiwan, ROC. Fax: +886 37 586 459.
E-mail address: bogun@nhri.org.tw (G.-G. Liou).
[1] These authors contributed equally to this work.

0006-291X/$ - see front matter © 2013 Elsevier Inc. All rights reserved.
http://dx.doi.org/10.1016/j.bbrc.2013.08.083

2. Materials and methods

2.1. Protein purification, gel filtration chromatography, gel electrophoresis, and Western blot

The preparative method of protein samples was described as previously [20] with some modifications. Briefly, His-tagged Spry2 was expressed in yeast cells (BJ459: SF10, MATa ura3-52 trp1 lys2-801 leu2Δ1 pep4Δ::HIS3 prb1Δ1.6R can1), successively purified through stepwise elution on a Ni^{2+}–NTA affinity column, and then subjected to gel filtration chromatography on a Superdex 200 column performed on an AKTA FPLC system (GE Healthcare). The fractionized protein samples were separated on either SDS–PAGE or native gels as indicated and were stained with Coomassie brilliant blue R520 to visualize the protein bands. The Western blots were performed using either the Immobilon Western detection system (Millipore) or the Western Lightning Plus-ECL reagent (PerkinElmer Life Sciences).

2.2. Negative staining, single particle reconstruction, and energy dispersive spectrum

For negative staining, 3 μl of the protein sample was adsorbed to a glow-discharged 200-mesh copper grid covered with carbon-coated collodion film, washed with three drops of distilled water, and stained with two drops of 0.75% uranyl formate. The samples were examined using an FEI Tecnai T12, a Hitachi H7650, a Jeol 1400, or a Jeol 2100F electron microscope.

For the 3D reconstitution, the images were recorded at a magnification of 52,000X and a defocus value of −1.5 μm using low-dose procedures on an FEI Tecnai T12 EM. The micrographs were digitized with a Zeiss/Integraph scanner using a step size of 14 μm, which corresponds to 3.5 Å on the object scale. A total of 10,690 Spry2 particle pairs were selected from 54-pair micrographs using the WEB program associated with the SPIDER software, which was used for the subsequent image-processing steps. The selected Spry2 particles were windowed into individual 90- × 90-pixel images and subjected to 10 rounds of multireference alignment and K-means classification with 40 output classes. The particles from those classes that showed almost the same projection average were combined. The particle images from the images of the titled micrographs were then used to calculate the 3D reconstitution model using the back-projection algorithm implemented in SPIDER. The orientation parameters of the particles were improved over eight refinement cycles using all of the images of the titled micrographs and 10% of the particles from the images of the untitled micrographs.

To obtain the energy dispersive spectrum (EDS), the sample preparation procedure was the same as that used for the negative staining, and the elemental analyses were performed using a Hitachi H7650 or a Jeol 1400 equipped with an EDS detector.

2.3. BIAcore surface plasmon resonance analysis

The real-time protein–protein interactions were monitored as described previously [20] with some modifications. Briefly, Spry2 and BSA were individually immobilized on different flow cells of a CM5 sensor chip using an amine-coupling kit (GE Healthcare/BIAcore). The concentrations of Spry2 and BSA used for the immobilization were 75 μg/ml, and the pH of the coupling buffer was 5.0 after the standard step of preconcentration was successfully performed. Using several different regeneration buffers, the un-chemical coupled Spry2 molecules of oligomers were then disassociated and washed out. The assays were performed on a BIAcore 2000 instrument with a constant flow rate (15 μl/min) at 20 °C. Varying concentrations of purified Spry2 ranging from 10 to 1000 nM were injected as the analytes. The chemical binding groups were regenerated by sequentially washing out the analytes with 15-μl injections of 0.1 M NaOH and 0.1% SDS until a background level was attained. The sensorgrams were subjected to global analysis using the BIA evaluation software 3.1. The global fitting analyzed the association and dissociation data obtained for the ligand–analyte interactions.

2.4. Electric resistance measurement

Purified Spry2 was dialyzed against a pH either equal to (pI buffer, 10 mM Tris–HCl, pH = 8.78) or lower (non-pI buffer, 10 mM NaOAc, pH = 5.5) than its pI. Both ferritin and catalase (GE Healthcare/Amersham) were dissolved in their own pI buffers (10 mM NaOAc, pH = 5.5 or 5.8 for ferritin or catalase, respectively) or the non-pI buffer (10 mM Tris–HCl, pH = 8.78). The protein samples were individually injected into a glass capillary (1 cm in length) until it was full. The two probes of the galvanometer were then inserted into both ends of the glass capillary, and the tips of the probes were jammed approximately 1 mm from the end of both sides. The electric resistance values were recorded for further statistic analyses.

3. Results

3.1. Spry2 can self-assemble into distinct oligomeric forms

The size-exclusion gel filtration experiment revealed at least five elution peaks according to the UV (280 nm) trace curve of the FPLC profile (Fig. 1A), and all these peaks were found to contain purified Spry2 by SDS–PAGE (Fig. 1B) and by Western blot using an anti-Spry2 antibody (Fig. S1A). This result was implied that the purified native Spry2 might exist in several multimeric forms to form a size-heterogeneous population. To further analyze these different fractions, native polyacrylamide gel electrophoresis was used. As shown in Fig. 1C, according to the molecular mass, Spry2 migrated as several species in different peaks. Peak 1 contained a high-order oligomeric form of Spry2, whereas peak 2 contained a major population of the hexameric form of Spry2, and peak 3 was included the majority of the trimeric form of Spry2. However, peak 4 mainly contained a mixture of the trimeric and dimeric forms of Spry2, whereas a mixture population of the mono-, di-, and trimeric forms was present in peak 5.

We also noticed that there might also be some type of post-translational modifications or altered folding involved in the different migrations of the different oligomeric forms of Spry2 on the native gel (e.g., trimer in peak 3 vs. trimer in peak 4). These modifications might be related to the distinct "active/functional" and "inactive/pro-functional" forms. Because of the importance of Spyr2Y55 phosphorylation in the regulation of RTK signal transduction [9,13], the signal of tyrosine phosphorylation was detected in the purified Spry2 by Western blot using an anti-phosphotyrosine antibody (Fig. S1B). The results show that the tyrosine phosphorylation status was different in the different fractions, which indicates that the state of tyrosine phosphorylation might be different in the different Spry2 oligomers.

Furthermore, we confirmed the existence of multi-type particles of Spry2 oligomers by examining each elution peak through negative-staining electron microscopy. We observed that the images from the distinct elutionfractions of purified Spry2 revealed particles of heterogeneous size and shape (Fig. S2A–D). However, because the particles in peak 3 exhibited much similar morphological features (Figs. 1D and S2E–F), we chose to pursue it further.

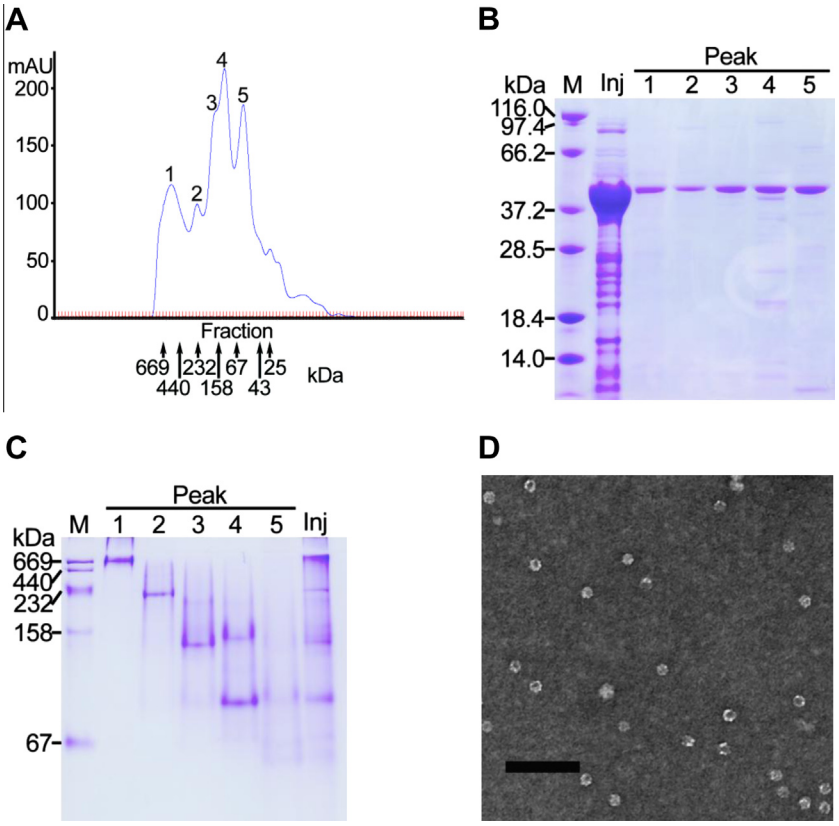

Fig. 1. Oligomeric forms of Spry2. (A) The elution profile of Spry2 obtained through in size-exclusion chromatography on a Superdex 200 gel-filtration column. The arrows on the fraction of the FPLC trace indicate the retention volume of the protein standards: 669 kDa, thyroglobulin; 440 kDa, ferritin; 232 kDa, catalase; 158 kDa, globulin; 67 kDa, albumin; 43 kDa, ovalbumin; and 25 kDa, chymotrypsinogen A. The fractions of peaks 1 through 5 were individually collected for the subsequent experiments. (B) Coomassie-stained SDS–polyacrylamide gel showing the purified Spry2 fractions of elution peaks 1 through 5. The protein standard markers (kDa) are labeled on the left side of the gel. (C) Coomassie-stained native polyacrylamide gel showing the migration of Spry2 as a mixture of oligomers. The molecular masses of the protein standards (kDa) and the fraction of the elution peak are indicated. (D) Electron micrograph showing the negatively stained purified Spry2 particles in peak 3. The bar represents 100 nm.

3.2. Spry2 self-interactions show a high kinetic affinity in vitro

To measure the real-time direct self-interactions of Spry2, we performed a BIAcore surface plasmon resonance (SPR) assay. Spry2 and BSA (for control) were individually immobilized on a CM5 sensor chip, and both proteins were also used as analytes. Subsequently, different concentrations of the analytes were individually injected over the chip surface, and the sensorgrams were recorded.

In these kinetic analyses, in general, the sensorgrams showed an initial rapid increase in the response units/signal upon Spry2 injection followed by the association of injected Spry2 with the Spry2 immobilized on the chip and then a slower association phase characteristic of Spry2 self-interactions, which resulted in a near plateau indicative of interaction saturation or equilibrium. After the injection of Spry2 as the analyte, the buffer was changed back to running buffer, and this change resulted in a rapid decrease in the response units/signal followed by the dissociation phase (Fig. 2A). The kinetic data of the on and off rates were estimated statistically, and the affinity calculation yielded KD values of approximately 16 nM for the Spry2 self-interactions (Fig. 2B).

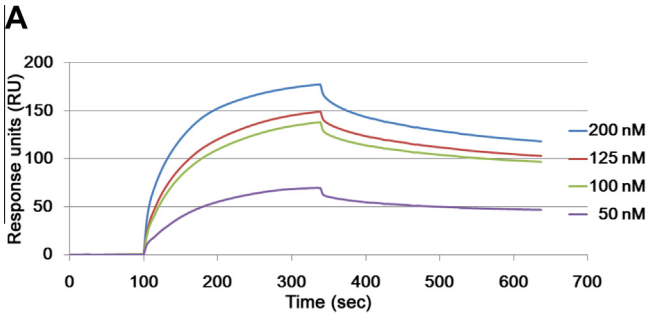

Fig. 2. Affinity of Spry2 self-interactions. (A) Representative sensorgrams of BIAcore SPR showing the binding of Spry2 to immobilized Spry2. The concentrations of Spry2 analytes are indicated on the sensorgrams (right). (B) Based on the BIAcore SPR experiments, the kinetic on (ka, M^{-1} s^{-1}) and off (kd, s^{-1}) rates and the calculated dissociation constants (KD, M) are summarized.

3.3. 3D structure of oligomeric Spry2 resembles a donut with two lip covers

For the 3D reconstitution of Spry2, we used the random conical tilt (CRT) approach [21] to calculate the 3D density map of Spry2 with a negative-staining method. Image pairs of the same specimen areas were recorded at an untilt angle of 0° and a tilt angle of 50° (Fig. S2E–F). We manually selected 10690 pairs of particles from 54 corresponding pairs of images using WEB, which is the display program associated with the SPIDER software package [22], and the particles from the images of the untilted specimens were classified into 40 classes using SPIDER (Fig. 3A). Many of these classes exhibited two-dimensional (2D) structural features that were very similar to those obtained with the negatively stained Spry2.

The 2D class averages showed that the shape of Spry2 resembles a ring with an additional seven knobs and likely a flexible connecting lobe on the inside to form an uncompleted-empty hole. The diameter of the ring shape was found to be approximately 15 nm.

We then combined the classes that showed the most similar features and performed the 3D reconstruction using all of the corresponding particles selected from the images of the tilted specimen and the best 10% corresponding particles selected from the images of the untilted specimen. The 3D reconstruction model of Spry2 showed that Spry2 can be easily configured as nine close lobe-domains and consists of a major central part and two lip-cover domains (Fig. 3B). The major central part appears to be donut-shaped with seven unequal petal-like lobes, whereas the lip-cover domains were individually and partially covered above both sides of the donut hole. The estimated resolution of the reconstitution density map was 25 Å according to the Fourier shell correlation = 0.5 criterion. The overall dimensions of the donut-like part exhibited an apparent thickness of approximately 4.2 nm, an internal diameter of approximately 5.0 nm, and external diameters of approximately 13.4 and 10.0 nm measured from two vertices or close points on the lobes. The connections of both lip-cover domains with the central donut-like part were not obviously detected by the 3D reconstitution. It is possible that the parts of the connection were conformationally flexible or non-rigid structures. In addition, these connections may be correlated with the change between the "active/functional" and "inactive/pro-functional" forms of Spry2.

3.4. Spry2 contains silicon and iron

The EDS analysis of the electron microscopy results was used to examine whether purified Spry2 contains any special element. Interestingly, the spectrum peaks revealed that the purified Spry2 contains both iron and silicon (Figs. 4A and S3A performed by different EMs for double confirmation). We noted that the buffer control or even the holder of the electron microscope occasionally resulted in a minor silicon signal, which can be ignored as background compared with the signals of Spry2 and with the signals of other proteins, such as ferritin and catalase (Fig. S3B–C). In addition, the total reflection X-ray fluorescence (TXRF) analysis performed on a S2 PICOFOX instrument also detected signals of silicon and iron in Spry2 (data not shown).

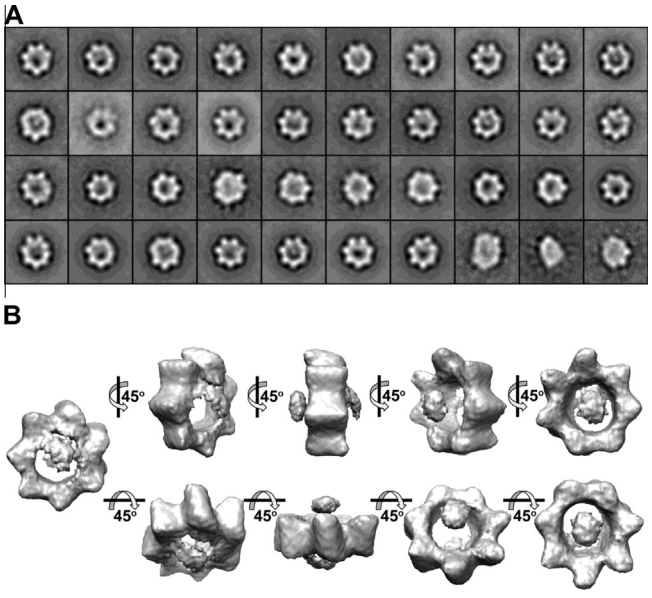

Fig. 3. Structure of Spry2. (A) Electron microscopy 2D projection averages of Spry2 particles from 40 classes. Each image average is shown in a 31.5- × 31.5-nm square. (B) Different views of the representative 3D reconstruction model of Spry2.

Spry2 has been shown to contain iron and is suggested to act as an intracellular nano-battery [23]. To the best of our knowledge, silicon has only been found in some plant cells and in the structural components of the shell or skeleton of aquatic organisms. Although silicon transporter proteins have been identified [24–28], there is no report regarding the existence of silicon and iron in any protein, and our result is the first report of a silicon- and iron-containing protein. However, the detailed molecular mechanism of the biological function of silicon in the protein still needs to be clarified.

3.5. Spry2 is able to serve as a biological material conductor

Silicon is known as one of the major elemental components of semiconductors. Because our results demonstrated that Spry2 contains silicon and iron, we hypothesized that Spry2 might play not only a bio-nano-battery role but also a bio-nano-semiconductor-like role to modulate the signal transduction between the molecules in the signaling pathway via its critical bio-nano-switch feature. Therefore, we used a galvanometer to examine whether the purified Spry2 in solution is capable of electroconductivity. To distinguish the contribution of silicon to the electroconductivity of Spry2, we also measured the electric resistance of an iron-carrier protein (ferritin) and a neither silicon nor metal ion chelated protein (catalase). The analytical conditions were their own isoelectric points (pIs) and non-pI valued buffers to avoid the possible effect of protein charge in the corresponding non-pI valued buffer. Interestingly, the electric resistance was markedly decreased when purified Spry2 was measured, regardless of whether it was measured in its pI (pH = 8.78) or non-pI (pH = 5.5) valued buffer, compared with the respective buffer controls (Fig. 4B). However, the electric resistance measurement of either ferritin or catalase in both their pI and non-pI valued buffers did not change significantly compared with the respective buffer control (Fig. 4B). These results indicate that the silicon in Spry2 is likely important for its electroconductivity, regardless of whether Spry2 is charged.

Theoretically, if the concentration of Spry2 in the solution is higher, it should provide a higher amount of mediators for electronic transport than those obtained at a lower concentration. In addition, the presence of additional electronic transportable mediators in the conductor should decrease the electric resistance. As expected, at least under the study conditions, i.e., within a range of 1 μM, the change in the electric resistance of Spry2 was found to be concentration-dependent (Fig. 4C). However, the correlation of the concentration and the electric resistance could not be simplified to a linear relationship. This relationship might be as complicated as a quadratic or a high-order curvilinear relationship. Thus, the details of this correlation require further investigation.

4. Discussion

In this study, we characterized the properties of Spry2 using several approaches. In summary, our results demonstrated that Spry2 in solution self-assembles into distinct oligomers, ranging from monomers, dimers, trimers to other higher-order oligomers. Nevertheless, it is unclear whether these different forms represent intermediate-assembly forms, functional/working forms, pro-functional/storage forms, and/or other processing forms for the distinct modulation roles in the relative signaling transduction regulation points.

The overall 3D structure model of Spry2 exhibited a donut-like shape with two loosely connecting lip-cover parts. The seven unequal-sized lobes of the donut and the two lip lobes, which partially covered both sides of the donut hole, are nine lobes in

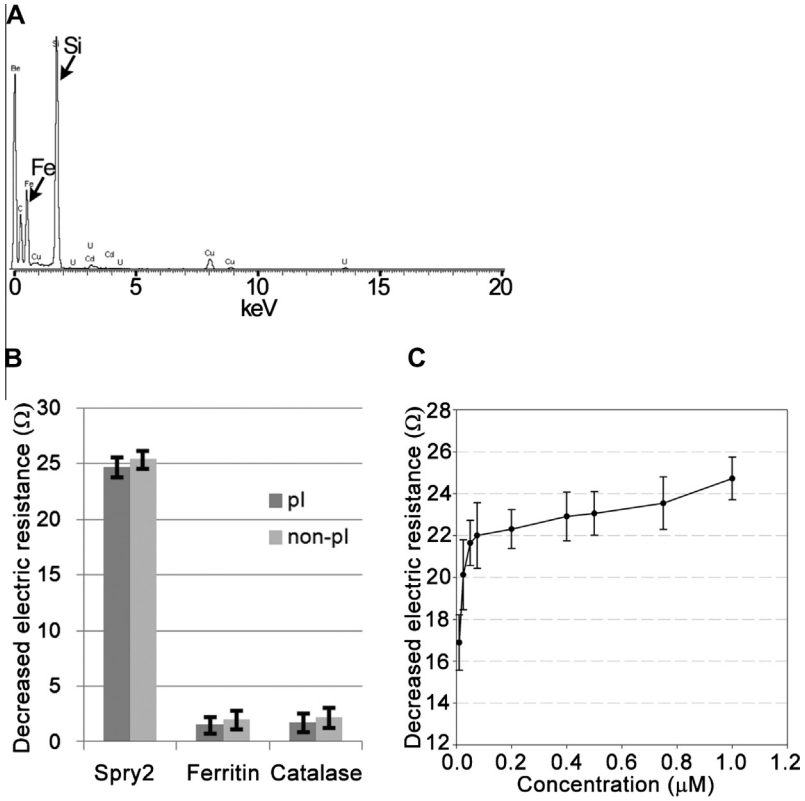

Fig. 4. Electroconductivity of Spry2. (A) The EDS of electron microscopy analysis was used to further examine the purified Spry2. The spectrum peaks represent and demonstrate that the purified Spry2 contains both iron and silicon. The major spectrum peaks represent iron and silicon, which are indicated as Fe and Si, respectively. (B) The changes in the electric resistance of Spry2, ferritin, and catalase in their own pI and non-pI valued buffers. (C) The changes in the electric resistance of Spry2 at different concentrations are plotted.

total. The nine lobes of the trimeric form are ideally and reasonably divided into three lobes in each Spry2 monomer. However, we do not know whether the two lip domains belong to a single Spry2 monomer or to two different monomers. One possibility is that the posttranslational modifications and/or elements (silicon and iron) contained within the monomers are different between the three monomers of the trimer and depend on which Spry2 monomer(s) form(s) the lip domain(s).

Spry2 was found to contain both iron and silicon, and the silicon present in Spry2 may contribute to the electroconductivity of Spry2. We propose that, in a cell, Spry2 may not only act as a bio-nano-battery but also play a bio-nano-semiconductor-like role to switch on or off the electronic transfer required for the modulation of signal transduction. However, it would be interesting to determine whether this critical bio-nano-switch feature is related to the loose connection of the lip-cover parts of the structure.

Our results also imply that Spry2 may be capable of being a potential native biological material that can be used as a conductor or even a semiconductor in the future. It is known that conventional high-performance physical electronic systems are built on the rigid and brittle planar surfaces of semiconductor wafers. The liquid crystal displays recently created a new material type of semiconductor devices. However, biological materials are soft, flexible, and elastic and also exhibit a curvilinear geometrical structural feature. In conclusion, our results indicate that it might be possible to develop another type of conductor or even semiconductor using either biological or half-biological hybrid materials.

Acknowledgments

We thank Yu-Ching Chen, Yi-Yun Chen, and the lab members of G.-G.L.'s lab for the technical help. We also thank the Institute of Molecular Biology, Academia Sinica (AS) for kindly providing an FEI Tecnai G2 EM, Dr. Chung-Shi Yang at the Center for Nanomedicine Research, NHRI for kindly providing a Hitachi H7650 EM, Dr. Wei-Hau Chang at the Institute of Chemistry, AS for kindly providing a Jeol 1400EM, and Dr. Yeu-Kuang Hwu at the Institute of Physics, AS and the National Synchrotron Radiation Research Center for kindly providing a Jeol 2100F EM to be used. This work was supported by grants MG-101-PP-08 and NSC-99-2311-B-400-002-MY3.

Appendix A. Supplementary data

Supplementary data associated with this article can be found, in the online version, at http://dx.doi.org/10.1016/j.bbrc.2013.08.083.

References

[1] K.G. Bache, T. Slagsvold, H. Stenmark, Defective downregulation of receptor tyrosine kinases in cancer, EMBO J. 23 (2004) 2707–2712.
[2] K. Haglund, P.P. Di Fiore, I. Dilic, Distinct monoubiquitin signals in receptor endocytosis, Trends Biochem. Sci. 28 (2003) 598–603.
[3] K. Haglund, S. Sigismund, I. Szymkiewicz, P.P. Di Fiore, I. Dikic, Multiple monoubiquitination of RTKs is sufficient for their endocytosis and degradation, Nat. Cell Biol. 5 (2003) 461–466.
[4] M. Ishida, M. Ichihara, S. Mii, M. Jijiwa, N. Asai, A. Enomoto, T. Kato, A. Majima, J. Ping, Y. Murakumo, M. Takahashi, Sprouty2 regulates growth and differentiation of human neuroblastoma cells through RET tyrosine kinase, Cancer Sci. 98 (2007) 815–821.
[5] J.M. Mason, D.J. Morrison, M.A. Basson, J.D. Licht, Sprouty protein: multifaceted negative-feedback regulators of receptor tyrosine kinase signaling, Trends Cell Biol. 16 (2006) 45–54.
[6] M.R. Schiller, Coupling receptor tyrosine kinases to Rho GTPaess-GEFs what's the link, Cell Signal. 18 (2006) 1834–1843.
[7] S.L. Schreiber, B.E. Bernstein, Signaling network model of chromatin, Cell 111 (2002) 771–778.
[8] M.M. McKay, D.K. Morrison, Integrating signals from RTKs to ERK/MAPK, Oncogene 26 (2007) 3113–3121.

[9] J.M. Mason, D.J. Morrison, B. Bassit, M. Dimri, H. Band, J.D. Licht, I. Gross, Tyrosin phosphorylation of Sprouty proteins regulates their ability to inhibit growth factor signaling: a dual feedback loop, Mol. Bio. Cell 15 (2004) 2176–2188.
[10] E.S. Wong, J. Lim, B.C. Low, Q. Chen, G.R. Guy, Evidence for direct interaction between Sprouty and Cbl, J. Biol. Chem. 276 (2001) 5866–5875.
[11] K. Haglund, M.H. Schmide, E.S. Wong, G.R. Guy, I. Dikic, Sprouty2 acts at the Cbl/CIN85 interface to inhibit epidermal growth factor receptor downregulation, EMBO Rep. 6 (2005) 635–641.
[12] A.B. Hall, N. Jura, J. DaSilva, Y.J. Jang, D. Gong, D. Bar-Sagi, HSpry2 is targeted to the ubiquitin-dependent proteasome pathway by c-Cbl, Curr. Biol. 13 (2003) 308–314.
[13] J.M. Mason, D.J. Morrison, B. Bassit, M. Dimri, H. Band, J.D. Licht, I. Gross, Tyrosine phosphorylation of Sprouty proteins regulates their ability to inhibit growth factor signaling: a dual feedback loop, Mol. Biol. Cell 15 (2004) 2176–2188.
[14] R.J. Nadeau, J.L. Toher, X. Yang, D. Kovalenko, R. Friesel, Regulation of Sprouty2 stability by mammalian seven-in-absentia homolog 2, J. Cell. Biochem. 100 (2007) 151–160.
[15] J. Qi, K. Nakayama, S. Gaitonde, J.S. Goydos, S. Krajewski, A. Eroshkin, D. Bar-Sagi, D. Bowtell, Z. Ronai, The ubiquitin ligase Siah2 regulates tumorigenesis and metastasis by HIF-dependent and -independent pathways, Proc. Natl. Acad. Sci. USA 105 (2008) 16713–16718.
[16] F. Edwin, K. Anderson, T.B. Patel, HECT domain-containing E3 ubiquitin ligase Nedd4 interacts with and ubiquitinates Sprouty2, J. Biol. Chem. 285 (2010) 255–264.
[17] G. Minowada, L.A. Jarvis, C.L. Chi, A. Neubuser, X. Sun, N. Hacohen, M.A. Krasnow, G.R. Martin, Vertebrate Sprouty genes are induced by FGF signaling and can cause chondrodysplasia when overexpressed, Development 126 (1999) 4465–4475.
[18] A.B. McKie, D.A. Douglas, S. Olijslagers, J. Graham, M.M. Omar, R. Heer, V.J. Gnanapragasam, C.N. Robson, H.Y. Leung, Epigenetic inactivation of the human sprouty2 (hSPRY2) homologue in prostate cancer, Oncogene 24 (2005) 2166–2174.
[19] M.J. Frank, D.W. Dawson, S.J. Bensinger, J.S. Hong, W.M. Knosp, L. Xu, C.E. Balatoni, E.L. Allen, R.R. Shen, D. Bar-Sagi, G.R. Martin, M.A. Teitell, Expression of sprouty2 inhibits B-cell proliferation and is epigenetically silenced in mouse and human B-cell lymphomas, Blood 113 (2009) 2478–2487.
[20] G.-G. Liou, J.C. Tanny, R.G. Kruger, T. Walz, D. Moazed, Assembly of the SIR complex and its regulation by o-acetyl-ADP-ribose, a product of NAD-dependent histone deacetylation, Cell 121 (2005) 515–527.
[21] M. Radermacher, T. Wagenknecht, A. Verschoor, F. Frank, Three-dimensional reconstruction from a single-exposure, random conical tilt series applied to the 50S ribosomal subunit of *Escherichia coli*, J. Microsc. 146 (1987) 113–136.
[22] F. Frank, M. Radermacher, P. Penczek, J. Zhu, Y. Li, M. Ladjadj, A. Leith, SPIDER and WEB: processing and visualization of images in 3D electron microscopy and related fields, J. Struct. Biol. 116 (1996) 190–199.
[23] X. Wu, P.B. Alexander, Y. He, M. Kikkawa, P.D. Vogel, S.L. McKnight, Mammalin sprout proteins assemble into large monodisperse particles having the properties of intracellular nanobatteries, Proc. Natl. Acad. Sci. USA 102 (2005) 14058–14062.
[24] J.F. Ma, K. Tamai, N. Yamaji, N. Mitani, S. Konishi, M. Katsuhara, M. Ishiguro, Y. Murata, M. Yano, A silicon transporter in rice, Nature 440 (2006) 688–691.
[25] J.F. Ma, N. Yamaji, N. Mitani, K. Tamai, S. Konishi, T. Fujiwara, M. Katsuhara, M. Yano, An efflux transporter of silicon in rice, Nature 448 (2007) 209–212.
[26] Y. Chiba, N. Mitani, N. Yamaji, J.F. Ma, HvLsi1 is a silicon influx transporter in barley, Plant J. 57 (2009) 810–818.
[27] N. Mitani, Y. Chiba, N. Yamaji, J.F. Ma, Identification and characterization of maize and barley Lsi2-Like silicon efflux transporters reveals a distinct silicon uptake system from that in rice, Plant Cell 21 (2009) 2133–2142.
[28] N. Mitani, N. Yamaji, Y. Ago, K. Iwasaki, J.F. Ma, Isolation and functional characterization of an influx silicon transporter in two pumpkin cultivars contrasting in silicon accumulation, Plant J. 66 (2011) 231–240.